Advances in Differential Equations and Control Processes 2026, 33(2), 3476.
doi: https://doi.org/10.59400/adecp3476

Article

A Haar wavelet operational matrix method for fractional Riccati differential equations with Atangana's beta derivative

Najeeb Alam Khan[1,*], Mumtaz Ali[1,2], Asmat Ara[1], Samreen Ahmed[1], Ali Saleh Alshomrani[3], Faris Alzahrani[3]

[1] Department of Mathematics, University of Karachi, Karachi 75270, Pakistan

[2] Department of Basic Sciences, Balochistan University of Engineering and Technology, Khuzdar 89100, Pakistan

[3] Mathematical Modeling and Applied Computation (MMAC) Research Group, Department of Mathematics, King Abdulaziz University, Jeddah 21589, Saudi Arabia

*** Corresponding authors:** Najeeb Alam Khan, njbalam@yahoo.com

CITATION

Khan NA, Ali M, Ara A, et al. A Haar wavelet operational matrix method for fractional Riccati differential equations with Atangana's beta derivative. Advances in Differential Equations and Control Processes. 2026; 33(2): 3476. https://doi.org/10.59400/adecp3476

ARTICLE INFO

Received: 1 July 2025
Revised: 18 May 2026
Accepted: 2 June 2026
Available online: 15 June 2026

Abstract: In this paper, we present an operational matrix method for integrating fractional Riccati differential equations (FRDEs) based on Haar wavelets. The fractional derivative is considered in the sense of Atangana's beta derivative, which effectively captures the memory and nonlocal characteristics of complex dynamical systems. The proposed technique employs a truncated Haar wavelet series and an operational matrix of integration to convert the governing FRDEs into a system of algebraic equations. These equations are then formulated as objective functions, and the unknown Haar wavelet coefficients are determined using a random search optimization procedure. This transformation reduces the computational complexity and provides an efficient framework for handling nonlinear fractional-order problems. The convergence and validity of the proposed method are demonstrated using several illustrative examples. The numerical results obtained with the proposed approach are compared with those from the Adams–Bashforth method, and the results show that the present technique provides more accurate approximations. Furthermore, to assess the performance and reliability of the method, several error metrics were computed, including the mean absolute deviation, root mean square error, Theil's inequality coefficient, Nash–Sutcliffe efficiency (NSE), and variance account for (VAF), for different numbers of collocation points. The results confirm that the Haar wavelet operational matrix method is simple to implement, computationally efficient, and highly accurate for solving fractional Riccati differential equations.

Keywords: operational matrix method; Haar wavelet; Atangana's beta derivative; fractional Riccati differential equations

1. Introduction

Fractional calculus (FC) is a mathematical concept that extends the notions of differentiation and integration to encompass non-integer-order systems. It has been extensively applied in modeling engineering and scientific problems, particularly in systems that exhibit memory, hereditary properties, and anomalous diffusion. Fractional differential and integral equations are crucial for describing a wide range of physical phenomena, including viscoelastic materials, fluid dynamics, signal processing, control theory, bioengineering, and financial modeling. In recent years, researchers have focused on developing analytical and numerical techniques to solve these problems. However, owing to their nonlocal nature and inherent

complexity, obtaining closed-form analytical solutions for most fractional equations is challenging. Consequently, there has been significant interest in developing reliable and efficient numerical methods for solving such problems. Several numerical methods have been proposed, such as the homotopy perturbation (HPM) [1], the variational iteration method (VIM) [2], Adomian decomposition method (ADM) [3], homotopy analysis method (HAM) [4], and different wavelet methods, such as the Legendre wavelet [5, 6], ultrasperical wavelet [7, 8], and Bernoulli wavelet [9]. Additionally, other approaches, including finite difference methods, spectral methods, collocation techniques, operational matrix methods, and optimization-based algorithms, have been widely used to approximate the solutions of fractional differential equations (FDEs). These techniques aim to transform the original fractional problem into a system of algebraic equations that can be solved efficiently using numerical procedures. Despite these advancements, there remains a need for more accurate, stable, and computationally efficient techniques that can handle nonlinear fractional models. Therefore, the development of improved numerical strategies remains an active area of research in FC and its applications in engineering.

The Riccati equation significantly influences various fields of engineering and applied research, including transmission line phenomena, diffusion problems, random process theory, and optimal control theory. These equations naturally emerge in filtering theory, fluid mechanics, quantum mechanics, population dynamics, and financial mathematics, where nonlinear behavior is crucial for describing system dynamics. In control engineering, Riccati equations are prevalent in linear quadratic regulator (LQR) problems, optimal estimation, and robust control design, whereas in stochastic processes, they are frequently encountered in covariance analysis and state estimation. Additionally, Riccati-type equations are employed to model wave propagation, heat transfer, and chemical reaction systems, underscoring their versatility in representing nonlinear physical phenomena. The nonlinear structure of the Riccati equation renders it particularly significant for theoretical analyses and numerical computations. Although classical Riccati equations can occasionally be transformed into linear second-order differential equations, such transformations are not always straightforward, particularly in the presence of variable coefficients or non-linear forcing terms. The complexity increases further when fractional-order derivatives are incorporated, as fractional Riccati differential equations (FRDEs) introduce memory effects and nonlocal behavior into the model. These features enhance the modeling capabilities but also increase the problem's mathematical complexity. Consequently, the development of efficient numerical techniques for solving Riccati and FRDEs remains a vital and active area of research in applied mathematics and engineering sciences.

Hence, techniques have been developed to solve Riccati differential equations, including VIM [10], He's VIM [11], ADM [3], and HPM [12]. In addition, Yuttanan et al. [13] introduced fractional-order generalized Legendre wavelets (FOGLWs) to solve FRDEs. An exact formula for the Riemann–Liouville fractional integral operator of the FOGLWs was derived using a hypergeometric function. By employing this formulation and the properties of FOGLWs, the FRDE is reduced to a system of

algebraic equations that can be solved efficiently. The method provides highly accurate results, and numerical examples are presented to demonstrate its effectiveness. Singh et al. [14] investigated the behavior of a nonlinear FRDE involving the Caputo–Prabhakar derivative. An efficient computational approach based on a combination of the homotopy analysis method and Sumudu transform was employed to obtain the solution. The convergence and uniqueness of the proposed scheme were analyzed. Furthermore, numerical results were presented through graphical illustrations to demonstrate the reliability and effectiveness of the method for solving the mathematical model with Prabhakar-type memory. Mohammad [15] presented a numerical framework for solving fractal-type FRDEs using tight wavelet frames constructed from Coiflet scaling functions. A fractal-type fractional derivative based on integral operators was introduced to capture the self-similar characteristics of the fractal structures. The proposed method combines this derivative with an efficient computational scheme to obtain accurate numerical solution. The results demonstrate improved accuracy and computational efficiency compared with existing approaches, such as Legendre–Galerkin and spline-based methods. The effectiveness of this technique in handling complex fractional dynamics highlights its potential for application in various scientific and engineering problems. Momani et al. [16] employed an iterative reproducing kernel method to obtain the solutions for fractional Riccati differential equations (FRDEs). Hosseinnia et al. [17], Odibat and Momani [18], and Khan et al. [19] utilized the modified HPM to solve the same type of equation.

Wavelet bases have attracted considerable attention for obtaining approximate solutions of differential equations of both integer and fractional orders. Due to their ability to accurately represent complex functions, wavelets provide efficient numerical schemes with fast computational performance. Moreover, wavelets exhibit excellent properties for detecting singularities, irregular structures, and transient behaviors arising in differential equations. In general, wavelet-based numerical techniques for differential equations are constructed using either collocation or Galerkin formulations. Among various wavelet families, Haar wavelets (HWs) are the simplest orthogonal compactly supported piecewise constant functions. However, because Haar wavelets are not differentiable at their discontinuity points, they cannot be directly applied to certain classes of differential equations, including Riccati-type equations. Two major approaches have been proposed to overcome this limitation. The first approach regularizes Haar wavelets through spline interpolation. In this regard, Cattani [20] presented a numerical approximation framework for differential operators using Haar wavelet bases together with spline-based derivatives. Their study demonstrated that spline smoothing enables the effective computation of Haar wavelet derivatives and illustrated the applicability of the method through a linear diffusion equation. The second approach is based on the integral operational matrix technique introduced by Chen and Hsiao [21]. Later, Lepik [22, 23] further extended Haar wavelet techniques for solving various classes of differential equations. Recently, Haar wavelet methods have been successfully applied to fractional-order dynamical systems arising in scientific and engineering applications. For example, Ali et al. [24] proposed a fractional-order atmospheric model describing the coupled dynamics of permafrost

thawing, atmospheric temperature, and greenhouse gas concentration. The model was formulated using the Atangana–Baleanu–Caputo (ABC) fractional derivative to incorporate memory effects associated with climate dynamics. To solve the resulting nonlinear fractional differential system, an operational matrix corresponding to the AB fractional integral operator was developed using Haar wavelets. The resulting system was transformed into an optimization problem and solved through differential evolution to estimate the unknown Haar wavelet coefficients. Numerical comparisons with predictor–corrector and standard numerical methods confirmed the effectiveness, accuracy, and computational efficiency of the proposed approach. Furthermore, theoretical investigations established the existence, uniqueness, and error bounds of the obtained solutions. Similarly, Sylvia and Ghosh [25] examine a fractional-order chemical clock reaction model formulated with the Caputo derivative to capture memory effects in chemical dynamics. They applied the HW method using an operational matrix to transform the system into nonlinear algebraic equations, which were then solved in MATLAB. The results were validated against the Adams–Bashforth method (ABM) and compared with the spectral collocation approach. Their analysis showed that the method had good convergence, with errors decreasing as the resolution level increased. Error comparisons indicate that the HW method produces more accurate results than the spectral collocation technique and is closely aligned with the benchmark method. In addition, stability, existence, and uniqueness analyses confirmed that the obtained solutions were reliable and well-behaved. Overall, the study demonstrates that the HW approach is an efficient and accurate tool for modeling fractional chemical clock reaction systems. Additional findings in this area may also be located in Amin et al., Khashan et al., and Ahsan et al. [26–28].

Inspired by the aforementioned studies, this study presents notable mathematical and computational advancements that set it apart from existing methodologies. The primary contribution is the development of a HWOMM specifically formulated for Atangana's beta fractional derivative, which contrasts with the classical Caputo and Riemann–Liouville operators typically utilized in prior research. Unlike these traditional fractional derivatives, which often involve nonlocal operators and singular kernel structures that complicate analytical and computational processes, Atangana's beta derivative offers a relatively simple local fractional formulation. This characteristic facilitates the derivation of the corresponding fractional integration operational matrix and enables a more straightforward numerical implementation, while maintaining the essential fractional-order properties of the model. By deriving the corresponding fractional integration operational matrix within this framework, the FRDEs are transformed into objective functions, and unknown HW coefficients are determined through RSO. Unlike traditional HW technique, which typically rely on direct algebraic solvers or deterministic iterative schemes, the integration of RSO offers a flexible and efficient optimization-based strategy for addressing nonlinear systems and enhancing computational adaptability. Furthermore, the proposed semi-analytical method requires minimal computational effort due to the simplicity of the Haar basis functions, achieves high accuracy with relatively few collocation points, and is easily implementable in standard computational software. To further substantiate

the robustness of the method, rigorous convergence analysis and error estimation were conducted, and the numerical results obtained were compared with the exact solutions and the Adams–Bashforth Method (ABM) [29], demonstrating the reliability, correctness, and effectiveness of the proposed approach. Therefore, the novelty of this work lies not merely in the application of Haar wavelets but in the introduction of a new operational matrix under Atangana's beta framework, its coupling with random search optimization, and the provision of its theoretical and numerical validation for solving FRDEs. Finally, performance metrics were implemented to assess reliability and correctness.

The structure of this paper is organized as follows: In Section 2, essential concepts of Atangana's beta derivative and integral are presented. In Section 3, the HW basis, function approximation, construction of operational matrix for fractional order integration, implementation of HWOMM, and RSO are discussed. In Section 6, numerical results and comparisons with exact solutions and the ABM are discussed through illustrative examples. Finally, Section 7, concludes the paper with a summary of key findings and future research directions.

2. Essential concept of Atangana's beta derivative

Definition 1. *Let ξ be function, such that, $\xi : [a, \infty) \to R$. Then, the $\beta-$derivative of ξ is defined as follows [30]:*

$$ {}_{0}^{A}D_{\psi}^{\beta}\left(\xi(\psi)\right) = \lim_{\kappa \to 0} \frac{\xi\left(\psi+\kappa\left(\psi+\frac{1}{\Gamma(\beta)}\right)^{1-\beta}\right)-\xi(\psi)}{\kappa}, \tag{1} $$

for all $\psi \geq a, 0 < \beta \leq 1$. Then the limit of above function exists, ξ is says to be $\beta-$differentiable.

Definition 2. *Let $\xi : [a, \infty) \to R$ be a continuous function. We propose the Atangana's $\beta-$integral of ξ as follows [30]:*

$$ {}_{a}^{A}I_{\psi}^{\beta}\xi(\psi) = \int_{a}^{\psi} \left(\varsigma + \frac{1}{\Gamma(\beta)}\right)^{\beta-1} \xi(\varsigma)d\varsigma. \tag{2} $$

The operator introduced above acts as the inverse counterpart of the proposed $\beta-$derivative and is therefore referred to as the $\beta-$integral.

The following two theorems illustrate how Atangana's $\beta-$derivative can be integrated with the $\beta-$integral.

Theorem 1. *For every value of $\psi \geq a$, assuming ξ is a given function that is both continuous and differentiable}, the following holds:*

$$ {}_{0}^{A}D_{\psi}^{\beta}\left({}_{0}^{A}I_{\psi}^{\beta}\xi(\psi)\right) = \xi(\psi). \tag{3} $$

Proof. For complete proof see Atangana and Doungmo Goufo [30]. □

Theorem 2. *For any value of $\psi \geq a$ with ξ is a specified function that is continuous*

and differentiable, we have:

$$ {}_{a}^{A}I_{\psi 0}^{\beta}\,{}_{\psi}^{A}D_{\psi}^{\beta}\xi(\psi) = \xi(\psi) - \xi(a). \tag{4}$$

Proof. For complete proof see Atangana and Doungmo Goufo [30]. □

3. Haar wavelets and function approximation

HWs are one of the simplest and earliest wavelet families used for function approximations and numerical analyses. They consist of piecewise constant basis functions generated by the dilation and translation of a single mother wavelet, which makes them computationally efficient and easy to implement. Haar wavelets were introduced in 1910 by the Hungarian mathematician Alfréd Haar and later became an important tool in numerical analysis, signal processing, and solving differential equations. In this section, the HWs and fractional integration matrix of HWs are discussed.

3.1. Haar wavelets

For $\psi \in [0,1]$, the HW functions can be described as follows [31]:

$$h_0(\psi) = \begin{cases} 1,\ \psi \in\ [0,1)\,, \\ 0, otherwise, \end{cases} \tag{5}$$

and,

$$h_i(\psi) = \begin{cases} 1 \text{ if } \frac{\sigma}{2^j} \le \psi < \frac{\sigma+0.5}{2^j}, \\ -1 \text{ if } \frac{\sigma+0.5}{2^j} \le \psi < \frac{\sigma+1}{2^j} \\ 0,\ \text{otherwise}, \end{cases}, \tag{6}$$

where the integers 2^j, $j = 0, 1, 2, 3, ..., J$, $J \in N$, denote the level of wavelets and the integers $\sigma = 0, 1, 2, ..., 2^j - 1$, are the translation parameters. The index i in Equation (6) is evaluated using $i = 2^j + \sigma + 1$. The minimal value of i is 2 and the maximal value of i is $M = 2^{J+1}$.

3.2. Approximation of square integrable function

Any function $\xi(\psi) \in L_2(\ [0,1))$ can be expanded in terms of HWs as:

$$\xi(\psi) = \varpi_1 h_1(\psi) + \varpi_2 h_2(\psi) + \varpi_3 h_3(\psi)... \tag{7}$$

If we consider $\xi(\psi)$ to be a piecewise constant function, the infinite series mentioned above can be expressed as a truncated series.

$$\xi(\psi) \approx \sum\nolimits_{i=1}^{M} \varpi_i h_i(\psi). \tag{8}$$

The matrix form of Equation (8) is:

$$\Psi = B^T H, \tag{9}$$

where $B^T = [\varpi_1, \varpi_2, ..., \varpi_M]$, is the row vector and Ψ is the discrete form of the

function $\xi(\psi)$. $H = [h_1(\psi), h_2(\psi), h_3(\psi), ..., h_M(\psi)]^T$ is the HW matrix of order M.

For instance, when $J = 2$ the HW matrix can be written as:

$$H_{8\times 8} = \begin{bmatrix} 1 & 1 & 1 & 1 & 1 & 1 & 1 & 1 \\ 1 & 1 & 1 & 1 & -1 & -1 & -1 & -1 \\ 1 & 1 & -1 & -1 & 0 & 0 & 0 & 0 \\ 0 & 0 & 0 & 0 & 1 & 1 & -1 & -1 \\ 1 & -1 & 0 & 0 & 0 & 0 & 0 & 0 \\ 0 & 0 & 1 & -1 & 0 & 0 & 0 & 0 \\ 0 & 0 & 0 & 0 & 1 & -1 & 0 & 0 \\ 0 & 0 & 0 & 0 & 0 & 0 & 1 & -1 \end{bmatrix}. \tag{10}$$

To obtain a numerical approximation of the function $\xi(\psi)$, we use the collocation points (CPs):

$$\psi_s = \frac{2s-1}{2M}, \;\; s = 1, 2, 3, ...M. \tag{11}$$

3.3. Operational matrix of fractional order integration of HWs

The integration of $H_M(\psi) = [h_1(\psi), h_2(\psi), h_3(\psi), ..., h_M(\psi)]^T$ can be approximated as follows [21]:

$$\int_0^{\psi} H_M(\tau)d\tau \cong P_{M\times M} H_M(\psi). \tag{12}$$

Matrix P, which is an M square, is known as the HWOMM of integration [21]. We aim to calculate the HWOMM for the fractional order integration. To achieve this objective we present the definition of fractional order integration [30], known as Atangana's $\beta-$fractional integration.

$$P^{\beta} H_M(\psi) = I^{\beta} H_M(\psi) = \left[I^{\beta} h_1(\psi), I^{\beta} h_2(\psi), I^{\beta} h_3(\psi), ..., I^{\beta} h_M(\psi)\right]^T,$$

$$= \left[\int_0^{\psi} \left(t + \tfrac{1}{\Gamma(\beta)}\right)^{\beta-1} h_1(t)dt, \int_0^{\psi} \left(t + \tfrac{1}{\Gamma(\beta)}\right)^{\beta-1} h_2(t)dt, \int_0^{x} \left(t + \tfrac{1}{\Gamma(\beta)}\right)^{\beta-1} h_3(t)dt, ..., \int_0^{\psi} \left(t + \tfrac{1}{\Gamma(\beta)}\right)^{\beta-1} h_M(t)dt\right]^T,$$

$$= [Ph_1(\psi), Ph_2(\psi), Ph_3(\psi), ..., Ph_M(\psi)]^T,$$

where

$$Ph_0(\psi) = \frac{1}{\beta}\left(\left(\psi + \frac{1}{\Gamma(\beta)}\right)^{\beta} - \left(\frac{1}{\Gamma(\beta)}\right)^{\beta}\right), \tag{13}$$

and

$$Ph_s(\psi) = \begin{cases} 0, \; \psi \in \; [0, \frac{\sigma}{2^j}), \\ \frac{1}{\beta}\left(\left(\psi + \frac{1}{\Gamma(\beta)}\right)^{\beta} - \left(\frac{\sigma}{2^j} + \frac{1}{\Gamma(\beta)}\right)^{\beta}\right), \; \psi \in [\; \frac{\sigma}{2^j}, \frac{\sigma+0.5}{2^j}), \\ \frac{1}{\beta}\left(2\left(\frac{\sigma+0.5}{2^j} + \frac{1}{\Gamma(\beta)}\right)^{\beta} - \left(\psi + \frac{1}{\Gamma(\beta)}\right)^{\beta} - \left(\frac{\sigma}{2^j} + \frac{1}{\Gamma(\beta)}\right)^{\beta}\right), \; \psi \in [\; \frac{\sigma+0.5}{2^j}, \frac{\sigma+1}{2^j}), \\ \frac{1}{\beta}\left(2\left(\frac{\sigma+0.5}{2^j} + \frac{1}{\Gamma(\beta)}\right)^{\beta} - \left(\frac{\sigma}{2^j} + \frac{1}{\Gamma(\beta)}\right)^{\beta} - \left(\frac{\sigma+1}{2^j} + \frac{1}{\Gamma(\beta)}\right)^{\beta}\right), \; \psi \in [\; \frac{\sigma+1}{2^j}, 1). \end{cases} \tag{14}$$

If $\beta = 0.95$ and $J = 2$ then the matrix $I^{0.95}$ of the integration in Equations (13)

and (14) given as,

$$P^{0.95} = \begin{bmatrix} 0.0624 & 0.1869 & 0.3107 & 0.4338 & 0.5564 & 0.6786 & 0.8002 & 0.9215 \\ 0.0624 & 0.1869 & 0.3107 & 0.4338 & 0.4340 & 0.3118 & 0.1902 & 0.0689 \\ 0.0624 & 0.1869 & 0.1869 & 0.0624 & 0.0025 & 0.0025 & 0.0025 & 0.0025 \\ 0 & 0 & 0 & 0 & 0.0612 & 0.1834 & 0.1834 & 0.0622 \\ 0.0624 & 0.0624 & 0.0007 & 0.0007 & 0.0007 & 0.0007 & 0.0007 & 0.0007 \\ 0 & 0 & 0.0624 & 0.0624 & 0.0005 & 0.0005 & 0.0005 & 0.0005 \\ 0 & 0 & 0 & 0 & 0.0612 & 0.0613 & 0.0004 & 0.0004 \\ 0 & 0 & 0 & 0 & 0 & 0 & 0.0607 & 0.0608 \end{bmatrix}.$$

3.4. Implementation of HWOMM

The HWOMM for addressing FRDEs utilizes an indirect integration technique as opposed to direct differentiation. This approach is employed due to the fact that the derivatives of HW are nullified almost everywhere within the domain. As a result, the estimation of highest-order derivative of the unknown function in the equation is conducted using HWs. Subsequently, approximations for the unknown function and its lower-order derivatives are derived through integration. This section delineates the process for employing the HWOMM for FRDEs in the context of Atangana's $\beta-$derivative. Consider the following FRDEs [32]:

$$ {}_0^A D_\psi^\beta \xi(\psi) = f(\psi) + g(\psi)\xi(\psi) + h(\psi)\xi^2(\psi), 0 < \beta \leq 1,\ 0 \leq \psi \leq 1, \tag{15}$$

with initial condition (IC)

$$\xi(0) = \gamma,$$

where ${}_0^A D_\psi^\beta \xi(\psi)$ Atangana's fractional derivative [30], and we assume that functions f, g and h are continuous on the interval $[0, 1]$. Approximate the terms that include Atangana's fractional derivative in Equation (15) using HW series.

Let

$$ {}_0^A D_t^\beta \xi(\psi) = \sum\nolimits_{i=1}^{M} \varpi_i h_i(\psi) = B^T H_M(\psi), \tag{16}$$

Utilizing Atangana's $\beta-$integral operator to Equation (16), the following result is obtained:

$$\xi(\psi) = \xi(0) + \sum\nolimits_{i=1}^{M} \varpi_i P_i^\beta(\psi) = \gamma + B^T P^\beta H_M(\psi), \tag{17}$$

replacing Equations (16) and (17) into Equation (15), the resulting expression becomes:

$$B^T H_M(\psi) = f(\psi) + g(\psi)\left(\gamma + B^T P^\beta H_M(\psi)\right) + h(\psi)\left(\gamma + B^T P^\beta H_M(\psi)\right)^2, \tag{18}$$

Equation (18) contains unknown HW coefficients ϖ_s, which are obtained by formulating and minimizing the following objective function:

$$\boldsymbol{\Phi} = \frac{1}{M}\sum\nolimits_{s=1}^{M}\left(B^T H - \left(f(\psi) + g(\psi)\left(\gamma + B^T P^\beta H\right) + h(\psi)\left(\gamma + B^T P^\beta H\right)^2\right)\right)^2. \tag{19}$$

The unknown coefficients in Equation (19) are determined using the built-in RSO routine available in Mathematica 11 at the selected CPs. Once these coefficients are

obtained, they are substituted into Equation (17) to construct an approximate solution for Equation (15). Although the objective function is nonlinear, the accuracy and reliability of the computed coefficients are validated by comparing them with the exact solutions and benchmark results obtained using the ABM.

3.5. Random search optimization

In this study, RSO is utilized to ascertain the unknown Haar wavelet coefficients that emerge in the HWOMM. The selection of the RSO is justified by its simplicity, ease of implementation, and compatibility with the proposed numerical framework. Given that the resulting objective function is nonlinear and may encompass multiple local minima, a random search offers an appropriate derivative-free optimization strategy that does not require analytical gradient information and can effectively explore various regions of the search space. Compared to more systematic or advanced optimization algorithms, RSO integrates seamlessly with Mathematica's built-in optimization tools and provides reliable performance for the problem at hand. The random search algorithm generates a population of randomly selected initial points within the prescribed search bounds of the unknown coefficients and applies a local optimization technique to each starting point to converge toward the local minima [33]. The optimal solution is identified as the best local minimum among all the obtained solutions. In this study, the search bounds for the Haar wavelet coefficients are defined according to the feasible domain of the optimization problem, whereas the number of search points is chosen as $\min(10d, 100)$, where d denotes the total number of optimization variables. Consequently, the population size is directly determined by the number of unknown coefficients that must be estimated. The available local search methods include automatic and interior points. The default automatic method employs penalty terms to handle constraints and determines the minimum using unconstrained optimization techniques, whereas the Interior Point method is employed for nonlinear constrained optimization. The optimization process was terminated when the prescribed tolerance level was satisfied, with the constraint violation tolerance set to 0.001, ensuring the convergence of the numerical procedure. To examine the sensitivity to random initialization, repeated optimization runs were conducted, and consistent coefficient values and numerical solutions were obtained, demonstrating the robustness and stability of the proposed approach. Furthermore, to ensure the reproducibility of the reported results, the random number generator seed was fixed at RandomSeed = 0. The objective function was optimized using the built-in RSO routines available in Mathematica 11.0, with the parameter settings listed in **Table 1**.

Table 1. Random search parameter setting [33].

Option name	Default value	Description
"Initial points"	Default	Set of points for optimization process
"Method"	Default	Determines the minimization technique to be employed
"PenaltyFunction"	Default	A custom function used to penalize violate constraints
"PostProcess"	Default	Indicates whether to apply a local search algorithm after the main optimization
"RandomSeed"	0	Sets the initial value for random number generator to ensure reproducibility
"Searchpoints"	Default	Defines the number of points used to initiate local search procedures
"Tolerance"	0.001	Specifies the allowable margin for constraint violations

3.6. Convergence analysis of HWOMM under Atangana's beta integral

Lemma 1. *Assume that $\xi(\psi)$ is continuous and differentiable on $(0,1)$ and there exists a constant $L>0$ such that $\left|\xi'(\psi)\right| \leq L$ for all $\psi \in (0,1)$. Suppose $\xi_{HWOMM}(\psi)$ is the Haar approximation of $\xi(\psi)$ then [34]:*

$$\|\xi(\psi)-\xi_{HWOMM}(\psi)\|_2 \leq \frac{L}{\sqrt{3}M}. \tag{20}$$

Theorem 3. *Let $\xi(\psi)$ denote the exact solution of the FRDE, and assume that $\xi_{HWOMM}(\psi)$ represent its approximate solution obtained using HWOMM. Then the following inequality holds, describing the error bound between the exact and approximate solutions.*

$$\|\xi(\psi)-\xi_{HWOMM}(\psi)\|_2 \leq \frac{\Delta L}{\sqrt{2\beta-1}\sqrt{3}M}. \tag{21}$$

Where $\Delta = \left(\frac{1}{2\beta}\left(\left(1+\frac{1}{\Gamma(\beta)}\right)^{2\beta}-\left(\frac{1}{\Gamma(\beta)}\right)^{2\beta}\right)-\left(\frac{1}{\Gamma(\beta)}\right)^{2\beta-1}\right)^{\frac{1}{2}}$.

Proof. Using Equation (2) we obtain,

$$\xi(\psi)=\xi(0)+\int_0^{\psi}\left(\varsigma+\frac{1}{\Gamma(\beta)}\right)^{\beta-1}\xi(\varsigma)d\varsigma, \tag{22}$$

By subtracting the approximate solution $\xi_{HWOMM}(\psi)$ from $\xi(\psi)$ and carrying out the required simplifications, the following expression is obtained.

$$\xi(\psi)-\xi_{HWOMM}(\psi)=\int_0^{\psi}\left(\varsigma+\frac{1}{\Gamma(\beta)}\right)^{\beta-1}(\xi(\varsigma)-\xi_{HWOMM}(\varsigma))d\varsigma.$$

Now, utilizing Cauchy-Schwarz's inequality:

$$\begin{aligned}&\leq \left(\int_0^{\psi}\left(\varsigma+\tfrac{1}{\Gamma(\beta)}\right)^{2\beta-2}d\zeta\right)^{\frac{1}{2}}\left(\int_0^{\psi}\left(\xi(\varsigma)-\xi_{HWOMM}(\varsigma)\right)^2 d\zeta\right)^{\frac{1}{2}},\\ &\leq \tfrac{1}{\sqrt{2\beta-1}}\left(\left(\psi+\tfrac{1}{\Gamma(\beta)}\right)^{2\beta-1}-\left(\tfrac{1}{\Gamma(\beta)}\right)^{2\beta-1}\right)^{\frac{1}{2}}\|\xi(\psi)-\xi_{HWOMM}(\psi)\|_2,\end{aligned} \tag{23}$$

using Lemma 1, yields,

$$(\xi(\psi)-\xi_{HWOMM}(\psi)) \leq \tfrac{L}{\sqrt{2\beta-1}\sqrt{3}M}\left(\left(\psi+\tfrac{1}{\Gamma(\beta)}\right)^{2\beta-1}-\left(\tfrac{1}{\Gamma(\beta)}\right)^{2\beta-1}\right)^{\frac{1}{2}}, \tag{24}$$

Taking L^2 norm on both sides we obtain,

$$\|\xi(\psi)-\xi_{HWOMM}(\psi)\|_2 \leq \tfrac{L}{\sqrt{2\beta-1}\sqrt{3}M}\left\|\left(\left(\psi+\tfrac{1}{\Gamma(\beta)}\right)^{2\beta-1}-\left(\tfrac{1}{\Gamma(\beta)}\right)^{2\beta-1}\right)^{\frac{1}{2}}\right\|_2, \tag{25}$$

$$\|\xi(\psi)-\xi_{HWOMM}(\psi)\|_2 \leq \frac{\Delta L}{\sqrt{2\beta-1}\sqrt{3}M}. \tag{26}$$

Where $\Delta = \left(\frac{1}{2\beta}\left(\left(1+\frac{1}{\Gamma(\beta)}\right)^{2\beta} - \left(\frac{1}{\Gamma(\beta)}\right)^{2\beta}\right) - \left(\frac{1}{\Gamma(\beta)}\right)^{2\beta-1}\right)^{\frac{1}{2}}$.

As the wavelet level M approaches infinity, the approximate solution $\xi_{HWOMM}(\psi)$ progressively converges to exact solution $\xi(\psi)$.

This completes the proof. □

4. Adam-Bashforth method

In this section, we utilize the ABM [29] as a numerical approximation technique for solving FDEs involving the $\beta-$derivative, primarily for a comparative analysis. This explicit multistep approach approximates the solution by leveraging information from previously computed steps, rendering it suitable for examining the dynamic behavior of the fractional system. This method facilitates a direct step-by-step numerical integration of the given problem without necessitating its transformation into an algebraic system, thereby preserving the structure of the original equation. Consider the following differential equation:

$$ {}_0^A D_t^{\beta} \xi(\psi) = \Upsilon\left(\psi, \xi(\psi)\right), \ \psi \in [0, T]. \tag{27}$$

Applying the $\beta-$integral to Equation (28) yields the following result:

$$\xi(\psi) - \xi(0) = \int_0^{\psi} \left(\zeta + \frac{1}{\sqrt{\beta}}\right)^{\beta-1} \Upsilon\left(\psi, \xi(\psi)\right) d\varsigma. \tag{28}$$

Let define $\psi_n = nh$, where h is the step size and $n = 0, 1, 2, ...$ Then, at $\psi = \psi_n$, we have:

$$\xi\left(\psi_n\right) = \xi(0) + \int_0^{\psi_n} \left(\zeta + \frac{1}{\sqrt{\beta}}\right)^{\beta-1} \Upsilon\left(\psi, \xi(\psi)\right) d\varsigma, \tag{29}$$

and at $\psi = \psi_{n+1}$, we have:

$$\xi\left(\psi_{n+1}\right) = \xi(0) + \int_0^{\psi_{n+1}} \left(\zeta + \frac{1}{\sqrt{\beta}}\right)^{\beta-1} \Upsilon\left(\psi, \xi(\psi)\right) d\varsigma. \tag{30}$$

Now, subtracting Equation (29) from Equation (30), we obtain:

$$\xi\left(\psi_{n+1}\right) = \xi\left(\psi_n\right) + \int_{\psi_n}^{\psi_{n+1}} \left(\zeta + \frac{1}{\sqrt{\beta}}\right)^{\beta-1} \Upsilon\left(\psi, \xi(\psi)\right) d\varsigma. \tag{31}$$

Although various forms of interpolating polynomials may be employed in the derivation, we adopt the Lagrange interpolation polynomial in this work, expressed as follows:

$$p(\psi) = \frac{\psi - \psi_{n-1}}{\psi_n - \psi_{n-1}} \Upsilon\left(\psi_n, \xi_n\right) + \frac{\psi - \psi_n}{\psi_{n-1} - \psi_n} \Upsilon\left(\psi_{n-1}, \xi_{n-1}\right).$$

Thus,

$$\begin{aligned} \xi_{n+1} = \xi_n &+ \int_{\psi_n}^{\psi_{n+1}} \frac{\Upsilon(\psi_n, \xi_n)}{\psi_n - \psi_{n-1}} \left(\varsigma - \psi_{n-1}\right) \left(\zeta + \tfrac{1}{\sqrt{\beta}}\right)^{\beta-1} d\varsigma \\ &+ \int_{\psi_n}^{\psi_{n+1}} \frac{\Upsilon(\psi_{n-1}, \xi_{n-1})}{\psi_{n-1} - \psi_n} \left(\varsigma - \psi_n\right) \left(\zeta + \tfrac{1}{\sqrt{\beta}}\right)^{\beta-1} d\varsigma. \end{aligned}$$

$$\xi_{n+1} = \xi_n + \frac{\Upsilon(\psi_n,\xi_n)}{h}\int_{\psi_n}^{\psi_{n+1}}(\varsigma-\psi_{n-1})\left(\zeta+\frac{1}{\sqrt{\beta}}\right)^{\beta-1}d\varsigma$$
$$-\frac{\Upsilon(\psi_{n-1},\xi_{n-1})}{h}\int_{\psi_n}^{\psi_{n+1}}(\varsigma-\psi_n)\left(\zeta+\frac{1}{\sqrt{\beta}}\right)^{\beta-1}d\varsigma.$$

Therefore, the approximate solution is computed using the following step-by-step recursive formula.

$$\begin{aligned}\xi_{n+1} = \xi_n &+ \frac{\Upsilon(\psi_n,\xi_n)}{h\beta(\beta+1)}\left(\psi_n+\frac{1}{\sqrt{\beta}}\right)^{\beta}\left(\psi_{n-1}-h\beta+\frac{1}{\sqrt{\beta}}\right)\\ &+\left(\psi_{n+1}+\frac{1}{\sqrt{\beta}}\right)^{\beta}\left(2h\beta-\psi_{n-1}-\frac{1}{\sqrt{\beta}}\right)\\ &+\frac{\Upsilon(\psi_{n-1},\xi_{n-1})}{h\beta(\beta+1)}\left(\psi_{n+1}+\frac{1}{\sqrt{\beta}}\right)^{\beta}\left(\psi_n-h\beta+\frac{1}{\sqrt{\beta}}-\left(\psi_n+\frac{1}{\sqrt{\beta}}\right)^{\beta+1}\right).\end{aligned} \tag{32}$$

Equation (32) represents the two-step fractional ABM corresponding to Atangana's $\beta-$derivative for order $0<\beta\leq 1$.

5. Evaluation criteria

To evaluate the performance of the proposed method, the mean absolute deviation (MAD), root mean square error (RMSE), Theil's inequality coefficient (TIC), Nash–Sutcliffe efficiency (NSE), and variance account for (VAF) were mathematically defined as measures of the error between the approximate and exact solutions. These indicators were used to examine the accuracy and reliability of the method. The MAD and RMSE measure the average error, whereas the TIC is used to assess the closeness of the approximate solution to the exact solution. The ENSE and EVAF were employed to evaluate the efficiency and overall performance of the proposed technique. Smaller MAD, RMSE, and TIC values indicate better accuracy, whereas larger ENSE and EVAF values indicate improved performance. These measures were calculated for different numbers of collocation points to analyze the effectiveness of the proposed method.

$$L_{MAD} = \frac{1}{M}\sum_{i=1}^{M}\left|\xi_i-\xi_i'\right|,\ L_{RMSE} = \sqrt{\frac{1}{M}\sum_{i=1}^{M}\left(\xi_i-\xi_i'\right)^2}, \tag{33}$$

$$L_{TIC} = \frac{\sqrt{\frac{1}{M}\sum_{i=1}^{M}\left(\xi_i-\xi_i'\right)^2}}{\sqrt{\frac{1}{M}\sum_{i=1}^{M}\left(\xi_i\right)^2}+\sqrt{\frac{1}{M}\sum_{i=1}^{M}\left(\xi_i'\right)^2}}, \tag{34}$$

$$\text{NSE} = 1-\left(\frac{\frac{1}{M}\sum_{i=1}^{M}\left(\xi_i-\xi_i'\right)^2}{\frac{1}{M}\sum_{i=1}^{M}\xi_i-\frac{1}{M}\sum_{i=1}^{M}\left(\xi_i'\right)^2}\right),\ L_{ENSE} = \left|1-\text{NSE}\right|, \tag{35}$$

$$\text{VAF} = \left(1-\frac{\text{variance}\left(\xi_i-\xi_i'\right)}{\text{variance}\left(\xi_i\right)}\right)\times 100, L_{EVAF} = 100-\text{VAF}. \tag{36}$$

Where ξ_i and $\xi_i^{'}$ represent the exact and numerical results, M stands for the number of CPs and $R_c(M)$ denotes the rate of convergence defined by:

$$R_c(M) = \frac{log\left(\frac{E\left(\frac{M}{2}\right)}{E(M)}\right)}{log2}. \tag{37}$$

6. Results and discussion

In this section, we evaluate the effectiveness of the newly established method by applying it to the FRDEs. Furthermore, correctness is assessed by analyzing the outcomes of the performance metrics for various numbers of CPs.

Example 1. *Consider the FRDE [35]:*

$$_0^A D_\psi^\beta \xi(\psi) = 1 + \xi^2(\psi)\ 0<\beta \leq 1,\ 0 \leq \psi \leq 1, \tag{38}$$

where the IC is $\xi(0) = 0$. *For* $\beta = 1$ *the exact solution to Equation (38) is* $\xi(\psi) = tan\psi$.

Let

$$_0^A D_t^\beta \xi(\psi) = \sum\nolimits_{i=1}^{M} \varpi_i h_i(\psi), \tag{39}$$

Utilizing Atangana's $\beta-$*integral operator to Equation (39), the following result is obtained:*

$$\xi(\psi) = \xi(0) + \sum\nolimits_{i=1}^{M} \varpi_i P_i^\beta(\psi), \tag{40}$$

substituting Equations (39) and (40) into Equation (38), we get:

$$\sum\nolimits_{i=1}^{M} \varpi_i h_i(\psi) = C + \left(\sum\nolimits_{i=1}^{M} \varpi_i P_i^\beta h_i(\psi)\right)^2, \tag{41}$$

where $C = [1, 1, 1, ..., 1]$.

Equation (41) can also be written in matrix form as:

$$B^T H = C + B^T P^\beta H, \tag{42}$$

where $P^\beta H = \left[P_i^\beta h_i\left(\psi_s\right)\right]_{M\times M}$.

Equation (42) contains unknown HW coefficients ϖ_s, *which are obtained by formulating and minimizing the following objective function:*

$$\boldsymbol{\Phi} = \frac{1}{M}\sum\nolimits_{s=1}^{M}\left(B^T H - \left(C + B^T P^\beta H\right)\right)^2. \tag{43}$$

The unknown ϖ_s *in Equation (43) are acquired through RSO at CPs* $\psi_s,\ s = 1, 2, 3, ..., M$. *Using* ϖ_s *in Equation (40) we obtain the required solution of Equation (39).*

Example 2. *Consider the nonlinear FRDE [18]:*

$$_0^A D_\psi^\beta \xi(\psi) = 1 + 2\xi(\psi) - \xi^2(\psi), 0 < \beta \leq 1, 0 \leq \psi \leq 1, \tag{44}$$

with the initial conditions $\xi(0) = 0$*, having exact solution at* $\beta = 1$*, as:*

$$\xi(\psi) = 1 + \sqrt{2}Tanh\left[\sqrt{2}\psi + \frac{log\left(\frac{-1+\sqrt{2}}{1+\sqrt{2}}\right)}{2}\right].$$

Example 3. *Consider the nonlinear FRDE [32]:*

$${}_0^A D_\psi^\beta \xi(\psi) = \left(\psi^3 - \psi^2\right)\xi(\psi) - \xi^2(\psi) + 3\psi^2 - 2\psi, 0 < \beta \leq 1,\ 0 \leq \psi \leq 1, \quad (45)$$

with the initial condition (IC) $\xi(0) = 0$*, having exact solution at* $\beta = 1$*, as* $\xi(\psi) = \psi^3 - \psi^2$.

The HWOMM, which is an optimization technique inspired by the RSO, was employed to solve FRDEs. **Figure 1** depicts the variation in absolute errors across different resolution levels, specifically J = 2, 4, and 6. However, enhancing the resolution significantly diminishes the magnitude of these errors. Notably, the scenario with $J = 6$ yielded the smallest errors, thereby affirming the high accuracy and convergence of the proposed method. These results underscore that the numerical scheme becomes more reliable and efficient at higher resolution.

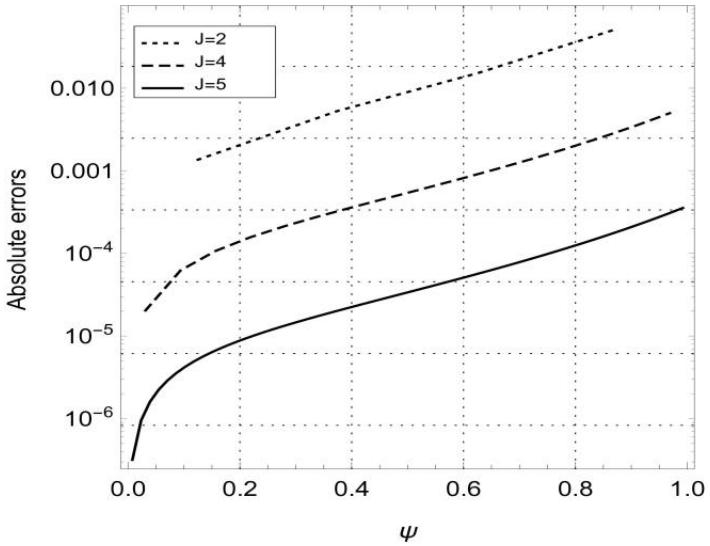

Figure 1. Absolute errors calculated for many values of J at $\beta = 1$ for Example 1.

Figure 2 present a comparison between the solutions obtained using the proposed HWOMM and the ABM for different fractional-order at $\beta = 0.95$ and $\beta = 0.9$. It can be observed that the numerical results produced by HWOMM closely coincide with ABM solutions over the entire computational domain. The overlap between the curves confirmed the high accuracy, stability, and reliability of the proposed approach. Moreover, the excellent agreement demonstrates that the HWOMM can efficiently approximate the solution with minimal deviation, validating its effectiveness in solving FDEs.

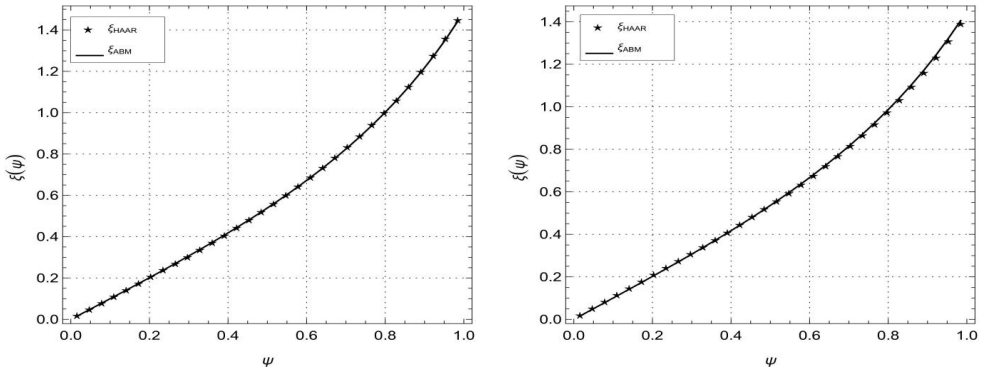

(a) **(b)**

Figure 2. **(a)** Comparison of HWOMM for $J = 4$ with ABM [29] at $\beta = 0.95$; **(b)** Comparison of HWOMM with ABM [29] at $\beta = 0.9$ for Example 1.

Similarly, **Figure 3** provide a comparison between the proposed HWOMM solution and the reference solutions obtained by the ABM for different parameter settings $\beta = 0.85$ and $\beta = 0.8$. It can be observed that the numerical results generated by HWOMM closely overlap with ABM solutions throughout the entire interval of ψ. The near coincidence of the curves confirmed the high accuracy, stability, and reliability of the proposed approach.

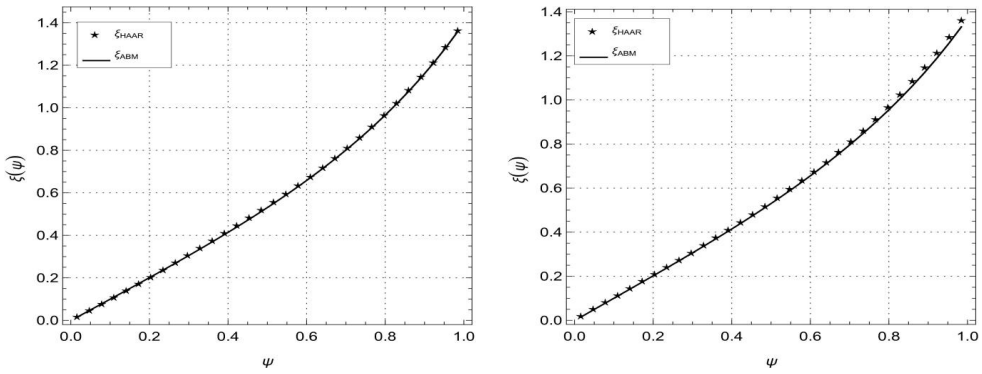

(a) **(b)**

Figure 3. **(a)** Comparison of HWOMM with ABM [29] at $\beta = 0.85$; **(b)** Comparison of HWOMM with ABM [29] at $\beta = 0.8$ for Example 1.

Table 2 compares the performance measures, convergence rate, and CPU time of HWOMM and ABM for Example 1. The results show that the error measures decrease significantly as number of CPs increases, confirming improved numerical accuracy for both methods. However, HWOMM consistently achieves smaller errors and a more stable convergence rate, approaching the ideal second order convergence 1.999, compared to ABM. Although CPU time of HWOMM is higher than that of ABM, the increased computational cost is justified by its superior accuracy and reliability. Overall, the results demonstrate that HWOMM provides a better balance between convergence performance and numerical precision.

Table 2. Comparison of the performance measures, convergence rate and CPU time (s) of HWOMM and ABM for Example 1.

				HWOMM			
J	L_{MAD}	L_{RMSE}	L_{TIC}	L_{ENSE}	L_{EVAF}	R_c	**CPU time (s)**
1	1.9318×10^{-2}	2.0200×10^{-2}	1.0717×10^{-2}	5.8665×10^{-3}	1.3686×10^{-2}	-	0.266
2	4.8294×10^{-3}	5.0587×10^{-3}	2.6831×10^{-3}	9.7223×10^{-5}	8.6113×10^{-4}	1.930	0.562
3	1.4930×10^{-3}	1.2071×10^{-3}	6.7094×10^{-4}	6.0314×10^{-6}	5.3925×10^{-5}	1.980	0.687
4	3.0177×10^{-4}	3.1628×10^{-4}	1.6774×10^{-4}	3.7626×10^{-7}	3.3720×10^{-6}	1.995	1.875
5	7.5443×10^{-5}	7.9071×10^{-5}	4.1936×10^{-5}	2.3505×10^{-8}	4.6923×10^{-8}	1.999	5.906
				ABM [29]			
J	L_{MAD}	L_{RMSE}	L_{TIC}	L_{ENSE}	L_{EVAF}	R_c	**CPU time (s)**
1	2.7354×10^{-2}	2.7809×10^{-2}	4.0840×10^{-2}	2.0546×10^{-2}	1.0656	-	0.006
2	1.5323×10^{-2}	2.3070×10^{-2}	1.5780×10^{-2}	3.0684×10^{-3}	1.7151×10^{-1}	0.988	0.020
3	9.1026×10^{-3}	6.7420×10^{-3}	6.1269×10^{-3}	4.6486×10^{-4}	2.7007×10^{-2}	1.111	0.030
4	1.5225×10^{-3}	2.0441×10^{-3}	1.3712×10^{-3}	2.3462×10^{-5}	1.3755×10^{-3}	2.026	0.040
5	3.4594×10^{-4}	1.1188×10^{-4}	3.6092×10^{-4}	1.6272×10^{-6}	9.5614×10^{-5}	1.852	0.050

Likewise, **Figure 4** presents the absolute error for various values of J at $\beta = 1$, for Example 2. **Figure 5** show a comparison between the HWOMM for $J = 4$ and the ABM [29] at $\beta = 0.95$ and $\beta = 0.9$, while, **Figure 6** display further comparisons between the proposed method for $J = 4$ and ABM [29] at $\beta = 0.85$ and $\beta = 0.8$.

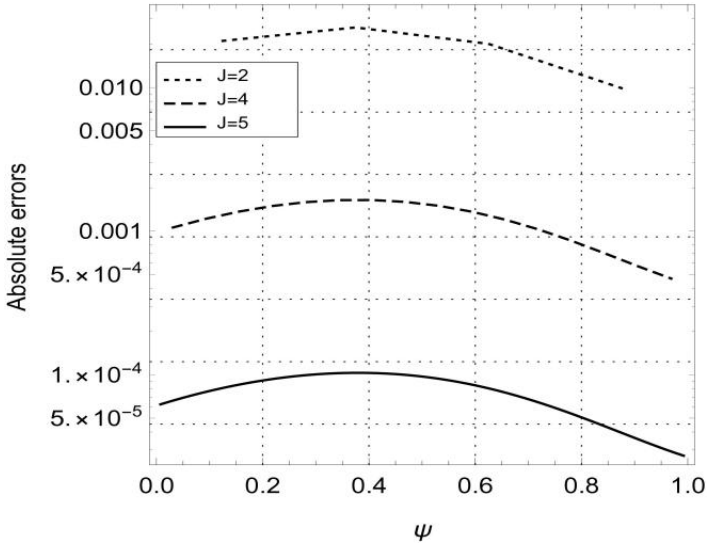

Figure 4. Absolute errors calculated for many values of J at $\beta = 1$ for Example 2.

Table 3 presents a comparative analysis of the performance metrics, convergence rate, and CPU time for the HWOMM and ABM in Example 2. The findings indicate a substantial reduction in all error metrics L_{MAD}, L_{RMSE}, L_{TIC}, L_{ENSE} and L_{EVAF} as the number of CPs increases, thereby confirming the robust convergence and enhanced approximation accuracy of both methodologies. The proposed HWOMM demonstrated reduced errors and more stable convergence behavior, with the convergence rate improving from 1.693 to 1.933, nearing second-order convergence. Although the CPU time for the HWOMM exceeds that of the ABM, the additional computational expense is warranted by its superior numerical accuracy and reliability. Overall, the results indicate that the HWOMM offers an effective balance between accuracy and computational efficiency.

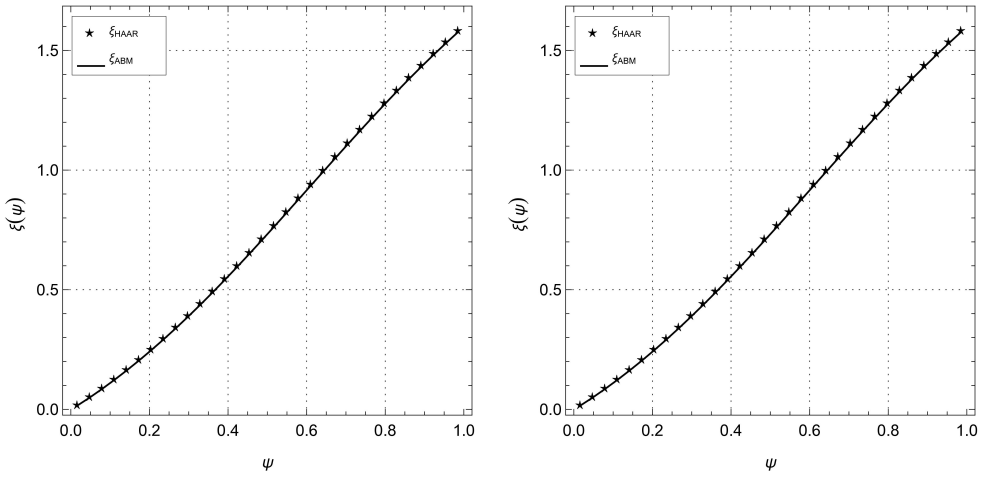

Figure 5. **(a)** Comparison of HWOMM for $J = 5$ with ABM [29] at $\beta = 0.95$; **(b)** Comparison of HWOMM for $J = 5$ with ABM [29] at $\beta = 0.9$ for Example 2.

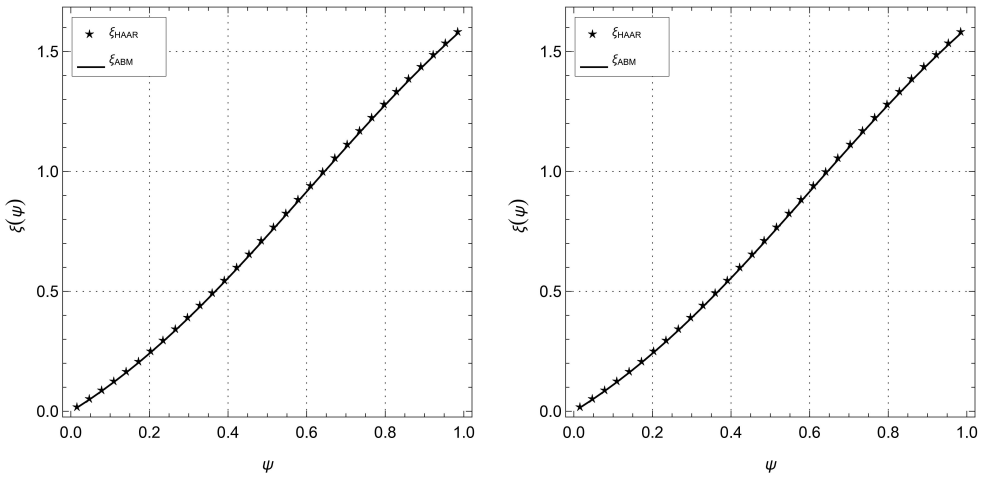

Figure 6. **(a)** Comparison of HWOMM for $J = 5$ with ABM [29] at $\beta = 0.85$; **(b)** Comparison of HWOMM for $J = 5$ with ABM [29] at $\beta = 0.8$ for Example 2.

Table 3. Comparison of the performance measures, convergence rate and CPU time (s) of HWOMM and ABM for Example 2.

				HWOMM			
J	L_{MAD}	L_{RMSE}	L_{TIC}	L_{ENSE}	L_{EVAF}	R_c	**CPU time (s)**
1	1.8526×10^{-2}	2.7354×10^{-2}	1.8435×10^{-2}	4.6848×10^{-3}	2.5358×10^{-1}	-	0.109
2	4.5839×10^{-3}	7.0663×10^{-3}	4.7405×10^{-3}	2.8779×10^{-4}	1.6668×10^{-2}	1.693	0.516
3	1.7842×10^{-3}	1.3342×10^{-3}	1.1954×10^{-3}	1.7861×10^{-5}	1.0528×10^{-3}	1.772	0.656
4	2.8565×10^{-4}	4.4725×10^{-4}	2.9956×10^{-4}	1.1231×10^{-6}	6.6500×10^{-5}	1.874	1.813
5	7.1403×10^{-5}	1.1188×10^{-4}	7.4933×10^{-5}	7.0199×10^{-8}	4.1610×10^{-6}	1.933	5.984
				ABM [29]			
J	L_{MAD}	L_{RMSE}	L_{TIC}	L_{ENSE}	L_{EVAF}	R_c	**CPU time (s)**
1	1.3613×10^{-2}	5.6545×10^{-2}	1.8986×10^{-2}	4.8781×10^{-2}	2.5408×10^{-1}	- 1.925	0.006
2	8.0307×10^{-2}	2.0678×10^{-3}	4.8918×10^{-3}	3.2141×10^{-4}	2.1391×10^{-2}	2.302	0.009
3	1.8513×10^{-3}	6.7420×10^{-3}	1.0969×10^{-3}	1.6114×10^{-5}	1.4686×10^{-3}	1.357	0.010
4	6.0012×10^{-4}	6.0012×10^{-4}	3.1823×10^{-4}	1.3546×10^{-6}	1.0579×10^{-4}	1.116	0.030
5	7.9071×10^{-4}	7.9071×10^{-5}	1.7899×10^{-4}	4.2833×10^{-7}	9.1970×10^{-6}		0.040

Table 4 presents a comparison of the absolute errors of the proposed HWOMM with Bernoulli wavelets (BWs) [9] the Müntz–Legendre Wavelet Collocation Method (MLWCM) [18] and Legendre wavelets (LWs) [36] for Example 2 at selected values of ψ. The results indicate that the HWOMM achieves significantly smaller absolute errors than the FBWs and FLWs across all tested points, thereby demonstrating a superior numerical accuracy. Compared with the ML Method, HWOMM provides competitive results, exhibiting comparable accuracy at most points. These findings confirm the effectiveness and reliability of the proposed HWOMM, underscoring its capability to produce highly accurate solutions and outperform several existing numerical methods in terms of accuracy. The HWOMM was also applied to other nonlinear FRDEs.

Table 4. Absolute error comparison of HWOMM with FBWs, ML Method and FLWs for Example 2.

ψ	HWOMM	BWs [9]	MLWCM [18]	FLWs [36]
0.1	6.2315×10^{-5}	2.9700×10^{-4}	1.0500×10^{-5}	1.1800×10^{-3}
0.2	7.9806×10^{-5}	7.8200×10^{-4}	1.5900×10^{-5}	1.4200×10^{-3}
0.3	1.0046×10^{-4}	1.9400×10^{-4}	9.3200×10^{-6}	1.9700×10^{-3}
0.5	8.6605×10^{-5}	1.2500×10^{-3}	6.5300×10^{-6}	2.4100×10^{-3}
1	2.7346×10^{-5}	2.7700×10^{-3}	1.2300×10^{-5}	3.8100×10^{-3}

In **Figure 7**, we observe the absolute errors for different values of J when $\beta = 1$. **Figure 8** depict a comparison between the proposed method for $J = 4$ and ABM [29] at $\beta = 0.95$ and $\beta = 0.9$. **Figure 9** depict a comparison between the proposed method for $J = 4$ and ABM [29] at $\beta = 0.85$ and $\beta = 0.8$.

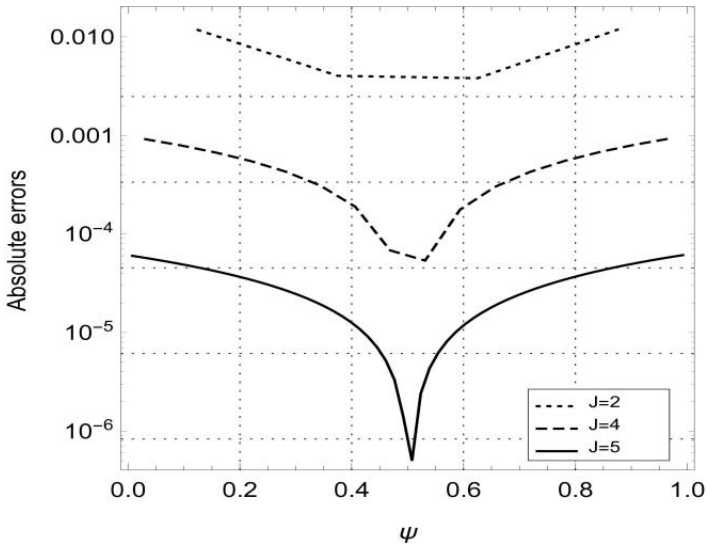

Figure 7. Absolute errors calculated for many values of J at $\beta = 1$ for Example 3.

The performance measures for Example 3 are listed in **Table 5**. Moreover, CPU time (in seconds) was calculated for each example, we computed the value of $R_c(M)$ for each example and determined from tables that it is about equivalent to 2. Therefore, we can infer that the HWOMM is a robust and efficient method for a numerical solving FRDEs.

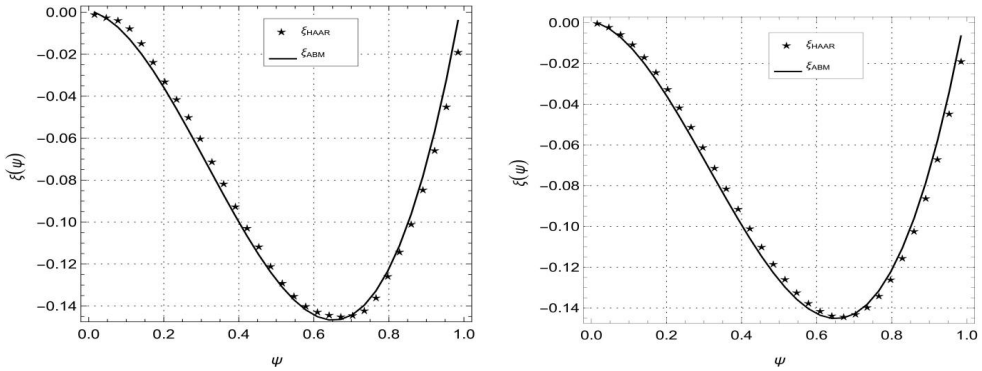

(a) **(b)**

Figure 8. **(a)** Comparison of proposed method for $J = 5$ with ABM [29] at $\beta = 0.95$; **(b)** Comparison of HWOMM for $J = 5$ with ABM [29] at $\beta = 0.9$ for Example 3.

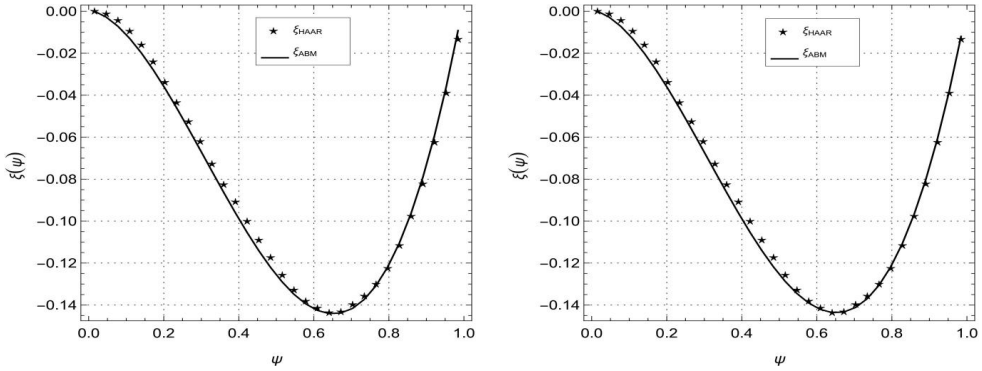

(a) **(b)**

Figure 9. **(a)** Comparison of HWOMM for $J = 5$ with ABM [29] at $\beta = 0.85$; **(b)** Comparison of HWOMM for $J = 5$ with ABM [29] a t$\beta = 0.8$ for Example 3.

Table 5. Comparison of the performance measures, convergence rate and CPU time (s) of HWOMM and ABM for Example 3.

				HWOMM			
J	L_{MAD}	L_{RMSE}	L_{TIC}	L_{ENSE}	L_{EVAF}	R_c	**CPU time (s)**
1	7.8503×10^{-3}	8.7809×10^{-3}	4.6848×10^{-2}	4.6848×10^{-3}	3.4316	-	0.094
2	1.9642×10^{-3}	2.2522×10^{-3}	1.1574×10^{-2}	9.7223×10^{-5}	2.0474×10^{-1}	1.767	0.454
3	4.9119×10^{-4}	5.6660×10^{-4}	2.9053×10^{-3}	1.2576×10^{-4}	1.2576×10^{-2}	1.898	0.594
4	1.2280×10^{-4}	1.4187×10^{-4}	7.8239×10^{-4}	7.8239×10^{-6}	7.8239×10^{-4}	1.952	1.438
5	3.0702×10^{-5}	3.5482×10^{-5}	1.8180×10^{-4}	4.8841×10^{-7}	4.8841×10^{-5}	1.977	4.703
				ABM [29]			
J	L_{MAD}	L_{RMSE}	L_{TIC}	L_{ENSE}	L_{EVAF}	R_c	**CPU time (s)**
1	2.2911×10^{-2}	2.3616×10^{-2}	1.1349×10^{-1}	2.4824×10^{-1}	2.4016×10^{-1}	-	0.00
2	1.3966×10^{-2}	1.6639×10^{-2}	8.3316×10^{-2}	1.1176×10^{-1}	1.1077×10^{-1}	1.225	0.001
3	7.6941×10^{-3}	9.4242×10^{-3}	4.7984×10^{-2}	3.2309×10^{-2}	1.1245×10^{-2}	2.210	0.01
4	4.2973×10^{-3}	5.3043×10^{-3}	2.7123×10^{-2}	1.0936×10^{-2}	2.1579×10^{-3}	1.357	0.020
5	2.9071×10^{-4}	2.7520×10^{-4}	1.4092×10^{-2}	2.9381×10^{-3}	3.2170×10^{-4}	1.563	0.030

7. Concluding remarks

In this study, we developed an operational matrix method based on HWs to effectively address FRDEs involving Atangana's $\beta-$derivatives. The proposed HWOMM was successfully applied to three representative FDEs, demonstrating its

robustness and applicability in the field. Comparisons with exact solutions, the ABM [29], and other recent numerical approaches confirmed the reliability and competitive performance of the proposed scheme. The observed convergence rates approached the ideal second-order convergence, reaching values of up to 1.999, which verified the strong convergence behavior and effectiveness of the HWOMM. Although the CPU time increased gradually with refinement, the computational cost remained acceptable relative to the substantial improvements in numerical accuracy. In addition, a convergence analysis of the HWOMM under Atangana's integral was conducted, providing theoretical support for the consistency and validity of the proposed method. This analysis confirmed that the approximation converged under suitable smoothness assumptions, thereby strengthening the mathematical foundation of the scheme. Despite these promising results, certain limitations should be acknowledged. Since Haar wavelets exhibit jump discontinuities, they are not differentiable at breakpoint locations, which may restrict their direct applicability in problems requiring higher-order smoothness. Moreover, because the Haar basis consists of piecewise constant functions, their classical derivatives vanish, making the formulation dependent on operational matrix representations. Achieving higher accuracy may also require a larger number of collocation points, which can increase computational complexity and optimization cost. Overall, the proposed HWOMM exhibits strong computational efficiency, accuracy, and theoretical reliability, making it a powerful tool for solving fractional-order models. The method developed in this study is not limited to the problems considered and can be extended to more complex partial FDEs arising in multidimensional physical and engineering systems in the future. Future research should focus on integrating the HWOMM with advanced swarm intelligence or evolutionary optimization algorithms to tackle more challenging models, including those involving variable-order fractional derivatives, time-delay effects, and nonlocal boundary conditions.

Authors contribution: Formulate the problem, NAK; methodology, NAK and AA; design the algorithm, NAK; software, FA; simulation, MA and ASA; validation, ASA; analysis, MA, ASA and FA; writing—original draft preparation, MA; writing—review and editing, AA and SA; visualization, SA and FA; supervision, NAK. All authors have read and agreed to the published version of the manuscript.

Funding: There is no funding reported for this work.

Institutional review board statement: Not applicable.

Informed consent statement: Not applicable.

Data availability statement: There is no data reported for this work.

Acknowledgement: The authors would like to thank the referees for their valuable comments that helped improve this paper.

Conflict of interest: All authors declare that there are no conflicts of interest.

AI use statement: The authors declare that no artificial intelligence (AI) tools were used in the preparation of the manuscript.

References

1. Nadeem M, He JH. The homotopy perturbation method for fractional differential equations: Part 2, two-scale transform. International Journal of Numerical Methods for Heat & Fluid Flow. 2022; 32(2): 559–567. doi: 10.1108/HFF-01-2021-0030
2. He JH, Latifizadeh H. A general numerical algorithm for nonlinear differential equations by the variational iteration method. International Journal of Numerical Methods for Heat & Fluid Flow. 2020; 30(11): 4797–4810. doi: 10.1108/HFF-01-2020-0029
3. Momani S, Shawagfeh N. Decomposition method for solving fractional Riccati differential equations. Applied Mathematics and Computation. 2006; 182(2): 1083–1092. doi: 10.1016/j.amc.2006.05.008
4. Fafa W, Odibat Z, Shawagfeh N. The Homotopy Analysis Method for Solving Differential Equations With Generalized Caputo-Type Fractional Derivatives. Journal of Computational and Nonlinear Dynamics. 2023; 18(2): 021004. doi: 10.1115/1.4056392
5. Singh AK, Mehra M. Wavelet collocation method based on Legendre polynomials and its application in solving the stochastic fractional integro-differential equations. Journal of Computational Science. 2021; 51: 101342. doi: 10.1016/j.jocs.2021.101342
6. Abbaszadeh D, Tavassoli Kajani M, Momeni M, et al. Solving fractional Fredholm integro–differential equations using Legendre wavelets. Applied Numerical Mathematics. 2021; 166: 168–185. doi: 10.1016/j.apnum.2021.04.008
7. Youssri YH. Orthonormal Ultraspherical Operational Matrix Algorithm for Fractal–Fractional Riccati Equation with Generalized Caputo Derivative. Fractal and Fractional. 2021; 5(3): 100. doi: 10.3390/fractalfract5030100
8. Shah FA, Abass R. Solution of fractional oscillator equations using ultraspherical wavelets. International Journal of Geometric Methods in Modern Physics. 2019; 16(05): 1950075. doi: 10.1142/S0219887819500750
9. Rahimkhani P, Ordokhani Y, Babolian E. A new operational matrix based on Bernoulli wavelets for solving fractional delay differential equations. Numerical Algorithms. 2017; 74(1): 223–245. doi: 10.1007/s11075-016-0146-3
10. Merdan M. On the Solutions Fractional Riccati Differential Equation with Modified Riemann-Liouville Derivative. International Journal of Differential Equations. 2012; 2012: 1–17. doi: 10.1155/2012/346089
11. Abbasbandy S. A new application of He's variational iteration method for quadratic Riccati differential equation by using Adomian's polynomials. Journal of Computational and Applied Mathematics. 2007; 207(1): 59–63. doi: 10.1016/j.cam.2006.07.012
12. Abbasbandy S. Homotopy perturbation method for quadratic Riccati differential equation and comparison with Adomian's decomposition method. Applied Mathematics and Computation. 2006; 172(1): 485–490. doi: 10.1016/j.amc.2005.02.014
13. Yuttanan B, Razzaghi M, Vo TN. Fractional-order generalized Legendre wavelets and their applications to fractional Riccati differential equations. International Journal of Nonlinear Sciences and Numerical Simulation. 2023; 24(1): 57–69. doi: 10.1515/ijnsns-2020-0137
14. Singh J, Gupta A, Kumar D. Computational Analysis of the Fractional Riccati Differential Equation with Prabhakar-type Memory. Mathematics. 2023; 11(3): 644. doi: 10.3390/math11030644
15. Mohammad M. A Tight Wavelet Frames-Based Method for Numerically Solving Fractional Riccati Differential Equations. Mathematical Methods in the Applied Sciences. 2025; doi: 10.1002/mma.10784
16. Momani S, Djeddi N, Al-Smadi M, et al. Numerical investigation for Caputo-Fabrizio fractional Riccati and Bernoulli equations using iterative reproducing kernel method. Applied Numerical Mathematics. 2021; 170: 418–434. doi: 10.1016/j.apnum.2021.08.005
17. Hosseinnia SH, Ranjbar A, Momani S. Using an enhanced homotopy perturbation method in fractional differential equations via deforming the linear part. Computers & Mathematics with Applications. 2008; 56(12): 3138–3149. doi: 10.1016/j.camwa.2008.07.002
18. Odibat Z, Momani S. Modified homotopy perturbation method: Application to quadratic Riccati differential equation of fractional order. Chaos, Solitons & Fractals. 2008; 36(1): 167–174. doi: 10.1016/j.chaos.2006.06.041
19. Khan NA, Ara A, Jamil M. An efficient approach for solving the Riccati equation with fractional orders. Computers & Mathematics with Applications. 2011; 61(9): 2683–2689. doi: 10.1016/j.camwa.2011.03.017
20. Cattani C. Haar Wavelet Splines. Journal of Interdisciplinary Mathematics. 2001; 4(1): 35–47. doi: 10.1080/09720502.2001.10700287
21. Chen CF, Hsiao CH. Haar wavelet method for solving lumped and distributed-parameter systems. IEE

Proceedings—Control Theory and Applications. 1997; 144(1): 87–94. doi: 10.1049/ip-cta:19970702
22. Lepik Ü. Numerical solution of differential equations using Haar wavelets. Mathematics and Computers in Simulation. 2005; 68(2): 127–143. doi: 10.1016/j.matcom.2004.10.005
23. Lepik Ü. Numerical solution of evolution equations by the Haar wavelet method. Applied Mathematics and Computation. 2007; 185(1): 695–704. doi: 10.1016/j.amc.2006.07.077
24. Ali M, Khan NA, Ayaz M, et al. Existence and uniqueness analysis of a fractional atmospheric system using Haar-based operational matrices. An International Journal of Optimization and Control: Theories & Applications (IJOCTA). 2025; 16(1): 91. doi: 10.36922/IJOCTA025320140
25. Sylvia J, Ghosh S. Numerical study of a chemical clock reaction framework utilizing the Haar wavelet approach. Journal of Mathematical Chemistry. 2025; 63(5): 1241–1286. doi: 10.1007/s10910-025-01719-8
26. Amin R, Patanarapeelert N, Barkat MA, et al. Two-dimensional Haar Wavelet Method for Numerical Solution of Delay Partial Differential Equations. Journal of Function Spaces. 2022; 2022: 1–9. doi: 10.1155/2022/7519002
27. Khashan MM, Amin R, Syam MI. A New Algorithm for Fractional Riccati Type Differential Equations by Using Haar Wavelet. Mathematics. 2019; 7(6): 545. doi: 10.3390/math7060545
28. Ahsan M, Bohner M, Ullah A, et al. A Haar wavelet multi-resolution collocation method for singularly perturbed differential equations with integral boundary conditions. Mathematics and Computers in Simulation. 2023; 204: 166–180. doi: 10.1016/j.matcom.2022.08.004
29. Akrami MH, Owolabi KM. On the solution of fractional differential equations using Atangana's beta derivative and its applications in chaotic systems. Scientific African. 2023; 21: e01879. doi: 10.1016/j.sciaf.2023.e01879
30. Atangana A, Doungmo Goufo EF. Extension of Matched Asymptotic Method to Fractional Boundary Layers Problems. Mathematical Problems in Engineering. 2014; 2014(1): 107535. doi: 10.1155/2014/107535
31. Yi M, Huang J. Wavelet operational matrix method for solving fractional differential equations with variable coefficients. Applied Mathematics and Computation. 2014; 230: 383–394. doi: 10.1016/j.amc.2013.06.102
32. Soleyman F, Area I. Müntz–Legendre Wavelet Collocation Method for Solving Fractional Riccati Equation. Axioms. 2025; 14(3): 185. doi: 10.3390/axioms14030185
33. Andradóttir S. Simulation optimization with countably infinite feasible regions: Efficiency and convergence. ACM Transactions on Modeling and Computer Simulation. 2006; 16(4): 357–374. doi: 10.1145/1176249.1176252
34. Ur Rehman M, Baleanu D, Alzabut J, et al. Green–Haar wavelets method for generalized fractional differential equations. Advances in Difference Equations. 2020; 2020(1): 515. doi: 10.1186/s13662-020-02974-6
35. Shameema V, Ranjini M. An operational matrix method for fractional differential equations with non-singular kernel. Journal of Fractional Calculus and Applications. 2023; 14(1): 157–170.
36. Ur Rehman M, Ali Khan R. The Legendre wavelet method for solving fractional differential equations. Communications in Nonlinear Science and Numerical Simulation. 2011; 16(11): 4163–4173. doi: 10.1016/j.cnsns.2011.01.014